

**DESIGN AND EVALUATION OF MR-SAFE LOADING
DEVICE FOR KNEE JOINT ASSESSMENT WITH MRI**

SANDEEP PANWAR JOGI



**CENTER FOR BIOMEDICAL ENGINEERING
INDIAN INSTITUTE OF TECHNOLOGY DELHI**

NOVEMBER 2022

© **Indian Institute of Technology Delhi (IITD), New Delhi, 2022**

**DESIGN AND EVALUATION OF MR-SAFE LOADING
DEVICE FOR KNEE JOINT ASSESSMENT WITH MRI**

by

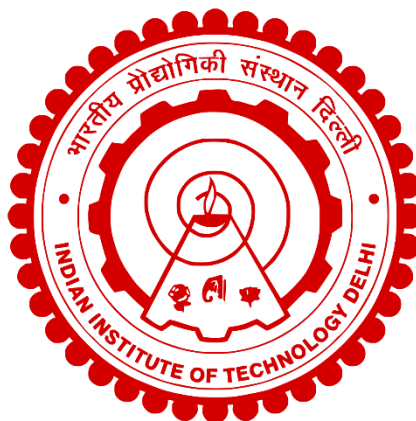
SANDEEP PANWAR JOGI

Center for Biomedical Engineering

Submitted

in fulfilment of the requirements of the degree of Doctor of Philosophy

to the



INDIAN INSTITUTE OF TECHNOLOGY DELHI

NOVEMBER 2022

Dedicated to,

Gurus, Parents, Wife, Shivansh, and Almighty God!

CERTIFICATE

This is to certify that the thesis entitled “**Design and Evaluation of MR-Safe Loading Device for Knee joint Assessment with MRI**”, being submitted by **Mr. Sandeep Panwar Jogi**, to the Indian Institute of Technology Delhi, for the award of ‘**Doctor of Philosophy**’ in Centre for Biomedical Engineering is a record of the bonafide research work carried out by him under our supervision and guidance. He has fulfilled the requirements for submission of this thesis, which to the best of our knowledge has reached the requisite standard. The material contained in the thesis has not been submitted in part or full to any other University or Institute for the award of any other degree or diploma.

Dr. Anup Singh

Associate Professor

Centre for Biomedical Engineering

Indian Institute of Technology Delhi

New Delhi – 110016, India

Dr. Amit Mehndiratta

Associate Professor

Centre for Biomedical Engineering

Indian Institute of Technology Delhi

New Delhi – 110016, India

Date:

New Delhi

Acknowledgments

Foremost, I would like to express my gratitude to my supervisors, Dr. Anup Singh and Dr. Amit Mehndiratta. The Hindi word “Guru” suited more than a guide for them. They have supervised me throughout my entire Ph.D. work. Their expertise in the knee joint MR parameters quantitative analysis and clinical experimental setup, that built the backbone of my thesis work. I would also like to thank them for the faith that they had shown in me during the entire course of my Ph.D. work. In short, they were my friend, philosopher, and guide (in reverse order) during the period of my Ph.D. I am thankful to my supervisor for embedding a holistic research aptitude, including statistical and mathematical analysis, mathematical modeling, hypothesis reframing, creativity, and scientific acumen. I also thank Dr. Sriram Rajan (Radiologist, Mahajan Imaging Center, New Delhi) for providing the much-needed clinical insight for my thesis work. More importantly, his scientific acumen and apt usage of language are something that I would like to inculcate all along.

Next, I would like to thank my respected research committee members for their feedback on my research work. I want to thank Dr. Deepak Joshi for his succinct suggestions and guidance throughout my Ph.D. I consider myself lucky enough to have a wonderful person like Dr. Sitikant Roy as my committee member. As the chairperson of my research committee, Dr. Harpal Singh provided me with the much-needed backing and encouragement required.

I want to thank Dr. Harsh Mahajan for providing MR imaging facilities at the imaging centers chain of Mahajan Imaging Center, New Delhi. I would like to thank Dr. Sriram Rajan, Dr. Vidur Mahajan and Dr. Vasantha Kumar Venugopala for their clinical insight and thought-provoking discussion. I admire Dr. Vidur Mahajan’s openness in talk and approach to taking prompt action. The candid approach of Dr. Vidur Mahajan and his team, especially Mrs.

Madhuri (Imaging Coordinator), Mr. Mandeep Singh, and Mr. Joseph(MR Technician), facilitate my Ph.D. work. I would like to thank Mr. Vishwajeet Singh (Ansys Inc., India), who helped to learn and run the FEA simulation.

I need to mention the faculties of IIT Delhi to help me strengthen the knowledge foundation to meet the research requirement. Especially, I would like to thank Dr. Arnab Chanda for inculcating the bottom-to-top approach of FEM using Ansys APDL.

I would be ungrateful not to mention the names of my immediate lab-mates who helped me variously during my Ph.D. Foremost, I would like to thank Dr. Rafeek Thaha, who worked with me shoulder-to-shoulder during my Ph.D. tenure. We used to work late at night during knee MRI scanning. We together were involved in data processing and visualization algorithm. I have to share uncountable technical discussions with Dr. Anirban, Dr. Ayan, Dr. Esha, Dr. Sneha, Dr.Rupsa, and Dr. Dinil. I would like to thank Archna and Dharmesh for continuously extending help in technical quires during My Ph.D. I shared the most thought-provoking sessions with Virender, Ankit, Himanshu, Rufia, Piyush, Ganesh, and Anshika. Apart, I thanks all for sharing the great memorable moment we lived in the MedImg Lab together.

My acknowledgment goes to some excellent teachers whose video courses have helped immensely in my Ph.D. Prof. Andrew Ng's course on Machine Learning and P.K Biswas's lecture on Image processing laid the foundation I needed during various phases of my Ph.D.

I am grateful to my funding agency IITD-IRD for providing research grants during my Ph.D. tenure. I would like to thank DST, the IIT research scholar fund, and CSIR for supporting my travel grant for attending conferences outside India.

Finally, I would like to mention my parents, wife, and son, who are the pillars of my life. I have only tried to walk on the footprints shown by them and find myself extremely blessed to have such a loving family by my side.

Sandeep Panwar Jogi

Abstract

The knee joint is one of the human body's largest and most complex joints. The functionalities of the joint depend on bones, muscles, ligaments, cartilage, meniscus, synovial fluid, and physiology. There could be various causes of ailment in the knee joint such as genetic factors, epigenetic factors, pathological conditions, fatigue, inflammation, and other biomechanical issues. This thesis included research studies on the tibiofemoral joint's weight-bearing soft-tissues (meniscus and cartilage).

Weight-bearing soft-tissues play a significant role in knee joint functionalities, whereas magnetic resonance imaging (MRI) is the gold-standard technique for imaging soft-tissues. Therefore, MRI is used as an imaging modality to assess the knee joints in this thesis. The routine knee joint MRI studies are conducted in a supine position, which overlooks the weight-bearing conditions of a joint. However, the changes in the joint could be dynamic that might be evident only during the weight-bearing condition, such as pain might arise during the loading conditions. Therefore, the knee joint's weight-bearing condition during scanning may represent *in-vivo* patho-physiological conditions. There are also reported diagnostic mismatches between unloaded and loaded knees during MRI. Therefore, the potential to get additional information from weight-bearing MRI to examine knee health is hypothesized in the thesis. Also, from a clinical perspective, load during imaging might potentially improve the diagnosis of knee health in the early stages.

There are various existing solutions for weight-bearing knee joint MRI. One of the solutions is open-standing MRI, but it suffers from a low signal-to-noise ratio (SNR). Besides, few other devices are available to exert load on the knee joint during MR scanning, but these devices have a bulky design, are expensive, and have a large setup time. Some of these devices

even require altering the MRI room settings. Further, the unidirectional loading mechanism of these devices potentially induce motion artifacts. Thus, these devices are not well suited for a busy clinical routine setup and confined to a research setting.

This thesis aims to develop a low-cost, lightweight, portable, and MR-safe knee joint axially loading device during MRI scanning, which addresses some of the limitations of the existing solution. Further, assess the device-induced change in MR parameters for knee joint characterization. Besides, this thesis also explores the further clinical applications of the weight-bearing knee MRI.

The first study in this thesis developed a low-cost, lightweight, portable knee joint axial loading device. Further, the developed device is calibrated and assessed for MR-safety, device-induced image artifacts, ease of doing, and degree of comfort for a subject. The device is developed in an iterative process with feedback from imaging partners and clinicians.

The objective of the second study of this thesis was to evaluate the developed device behaviors and the changes due to load in MR quantitative parameters for characterizing knee joint. This study consisted of two sub-studies: i) to compare the loading behavior of the developed device with natural standing stance using open-standing MRI 0.25 Tesla, and ii) to assess the MR parameter changes due to load using the developed device with 3.0 Tesla MRI. In the first sub-study, the tibiofemoral bone gap during the device load was compared to a natural standing load of various stances. The device exerted load was observed similar to a natural stance of standing with both (Pearson Coefficient ' r ' > 0.9). The loading effect on the change in bone gap, cartilage thickness, and cartilage T2-value was evaluated in the second sub-study; the observations are found to be similar to the previously reported research observations.

The third work in this thesis was on developing a novel method to estimate the subject-specific in-vivo stiffness of the tibiofemoral joint non-invasively. This study consisted of two sub-studies: experimental study and simulation study. In the experimental study, the MRI scanned images of a knee joint with and without load (using the developed loading device) were used to evaluate the mean tibiofemoral strain. In the simulation study, a subject-specific knee joint finite-element-analysis (FEA) was performed with varying tibiofemoral joint stiffness to develop the stiffness versus strain model. The subject-specific experimental strain was fed in the stiffness versus strain model to evaluate the subject-specific stiffness. Further, the thesis also presented a generalized mathematical model to estimate in-vivo tibiofemoral joint stiffness.

The research outcomes in this thesis might make the weight-bearing knee joint MRI more accessible. Further, this work might open new applications for weight-bearing MRI and expedite knee research.

सार

घुटने का जोड़ मानव शरीर के सबसे बड़े और सबसे जटिल जोड़ों में से एक है। जोड़ की कार्यक्षमता हड्डियों, मांसपेशियों, स्नायुबंधन, उपास्थि, मेनिस्कस, श्लेष द्रव और शरीर क्रिया विज्ञान पर निर्भर करती है। घुटने के जोड़ में बीमारी के कई कारण हो सकते हैं जैसे आनुवंशिक कारक, पश्चजनन सम्बन्धी कारक, रोग की स्थिति, थकान, सूजन और अन्य जैवयांत्रिकी मुद्दे। इस शोध प्रबंध में टिबिओफेमोरल (Tibiofemoral) जोड़ के भारोत्तोलन नरम-ऊतकों (मेनिस्कस और उपास्थि) पर शोध अध्ययन शामिल थे।

भार-वहन नरम-ऊतक घुटने के जोड़ की कार्यक्षमता में महत्वपूर्ण भूमिका निभाते हैं, जबकि मैग्नेटिक रेजोनेंस इमेजिंग (एमआरआई (MRI)) नरम-ऊतक की इमेजिंग के लिए स्वर्ण-मानक तकनीक है। इसलिए, इस शोध प्रबंध में, घुटने के जोड़ को अवेध्य रूप से आकलन करने के लिए एमआरआई(MRI) का उपयोग इमेजिंग तौर-तरीकों के रूप में किया जाता है। घुटने के जोड़ के नियमित एमआरआई अध्ययन एक उत्तम पड़ी हुई स्थिति में आयोजित किए जाते हैं, जो एक जोड़ की भार वहन करने वाली स्थितियों की अनदेखी करता है। हालांकि, जोड़ में परिवर्तन गतिशील हो सकते हैं जो केवल भार-वहन की स्थिति के दौरान स्पष्ट हो सकते हैं, जैसे कि भार वहन की स्थिति के दौरान दर्द उत्पन्न हो सकता है। इसलिए, क्रमवीक्षण के

दौरान घुटने के जोड़ की भार वहन करने वाली स्थिति जीवे विकृति-शारीरिक स्थितियों का प्रतिनिधित्व कर सकती है। एमआरआई (MRI) के दौरान गैर-भार-वहन और भार-वहन घुटनों के बीच नैदानिक बेमेल होने की भी सूचना है। इसलिए, शोध प्रबंध ने घुटने के स्वास्थ्य की जांच के लिए भारोत्तोलन एमआरआई(MRI) से अतिरिक्त जानकारी प्राप्त करने की क्षमता की परिकल्पना की है। इसके अलावा, नैदानिक दृष्टिकोण से, इमेजिंग के दौरान भार प्रारंभिक अवस्था में घुटने के स्वास्थ्य के निदान में संभावित रूप से सुधार कर सकता है।

वजन-वहन करने वाले घुटने के जोड़ के एमआरआई(MRI) के लिए कई मौजूदा समाधान हैं। समाधानों में से एक ओपन-स्टैंडिंग एमआरआई है, लेकिन यह कम सिग्नल-टू-शोर अनुपात (एसएनआर(SNR)) से ग्रस्त है। इसके अलावा, एमआर(MR) क्रमवीक्षण के दौरान घुटने के जोड़ पर भार डालने के लिए कुछ अन्य उपकरण उपलब्ध हैं, लेकिन इन उपकरणों का भारी डिज़ाइन है, महंगे हैं, और एक बड़ा स्थापित करने का समय है। इनमें से कुछ उपकरणों को एमआरआई (MRI) कमरे की स्थापना बदलने की भी आवश्यकता होती है। इसके अलावा, इन उपकरणों का एक-दिशात्मक भारोत्तोलन तंत्र संभावित रूप से गति विरूपण साक्ष्य को प्रेरित करता है। इस प्रकार, ये उपकरण एक व्यस्त नैदानिक दिनचर्या स्थापना के लिए उपयुक्त नहीं हैं और एक शोध-स्थापना तक ही सीमित हैं।

इस शोध प्रबंध का उद्देश्य एमआरआई स्कैनिंग के दौरान कम लागत वाला, हल्का, उठाऊ और एमआर(MR)-सुरक्षित घुटने का जोड़ अक्षीय भार उपकरण विकसित करना है, जो

मौजूदा समाधान की कुछ कमियों को दूर करता है। इसके अलावा, घुटने के जोड़ के लक्षण वर्णन के लिए एमआर(MR) मापदंडों में विकसित उपकरण-प्रेरित परिवर्तन का आकलन करने के लिए है। इसके अलावा, यह शोध प्रबंध भारोत्तोलन घुटने की एमआरआई(MRI) के भविष्य के नैदानिक अनुप्रयोगों की भी पड़ताल करती है।

इस शोध प्रबंध में पहले अध्ययन ने एक कम लागत वाला, हल्का, उठाऊ, घुटने के संयुक्त अक्षीय भार-वहन उपकरण का विकास किया। इसके अलावा, विकसित उपकरण को एमआर(MR)-सुरक्षा, उपकरण-प्रेरित छवि विरूपण साक्ष्य, करने में आसानी, और किसी विषय के लिए आराम की मापदंड के लिए अंश-शोधन और मूल्यांकन किया गया है। इमेजिंग भागीदारों और चिकित्सकों से प्रतिक्रिया के साथ इस उपकरण को एक पुनरावृत्त प्रक्रिया में विकसित किया गया है।

इस शोध प्रबंध के दूसरे अध्ययन का उद्देश्य विकसित उपकरण व्यवहार और घुटने के जोड़ की विशेषता वाले एमआर मात्रात्मक मापदंडों में भार के कारण होने वाले परिवर्तनों का मूल्यांकन करना था। इस अध्ययन को दो उप-अध्ययनों शामिल थे: i) ओपन-स्टैंडिंग 0.25 टेस्ला(Tesla) एमआरआई MRI का उपयोग करके, विकसित उपकरण से भार के व्यवहार की तुलना प्राकृतिक स्टैंडिंग स्टॉंस के साथ करना, और ii) 3.0 टेस्ला(Tesla) एमआरआई(MRI) के साथ विकसित उपकरण का उपयोग करके भार के कारण एमआर(MR) मापदंडों में परिवर्तनों का आकलन करना। पहले उप-अध्ययन में, उपकरण से भार के दौरान

टिबिओफेमोरल(Tibiofemoral) हड्डियों के अंतर की तुलना विभिन्न मुद्रा के प्राकृतिक रूप से खड़े होने क भार से की गई थी। उपकरण द्वारा लगाया गया भार दोनों पैर के साथ खड़े होने के प्राकृतिक रुख के समान देखा गया (पियर्सन गुणांक (Pearson's Coefficient) 'आर'('r') > 0.9)। दूसरे उप-अध्ययन में हड्डी के अंतर, उपास्थि की मोटाई और उपास्थि T2-मूल्य में परिवर्तन से भार के प्रभाव का मूल्यांकन किया गया था; अवलोकन पहले बताए गए शोध टिप्पणियों के समान पाए गया हैं।

इस शोध प्रबंध में तीसरा काम अवेध्य रूप से टिबिओफेमोरल संयुक्त की विषय-विशिष्ट जीवे कठोरता का अनुमान लगाने के लिए एक नव विधि के विकास पर था। इस अध्ययन में दो उप-अध्ययन शामिल थे: प्रायोगिक अध्ययन और अनुकरण अध्ययन। प्रायोगिक अध्ययन में, बिना भार और भार के साथ (विकसित भार-वहन उपकरण का उपयोग करके) घुटने के जोड़ की एमआरआई(MRI) क्रमवीक्षण की गई छवि का उपयोग माध्य टिबिओफेमोरल(Tibiofemoral) तनाव का मूल्यांकन करने के लिए किया गया था। अनुकरण अध्ययन में, एक विषय-विशिष्ट घुटने के संयुक्त परिमित-तत्व-विश्लेषण (FEA) को अलग-अलग टिबिओफेमोरल(Tibiofemoral) जोड़ की कठोरता के साथ कठोरता बनाम तनाव मॉडल विकसित करने के लिए किया गया था। विषय-विशिष्ट कठोरता का मूल्यांकन करने के लिए विषय-विशिष्ट प्रयोगात्मक तनाव को कठोरता बनाम तनाव तंत्र में डाला गया था। इसके

अलावा, शोध प्रबंध जीवे टिबिओफेमोरल(Tibiofemoral) संयुक्त कठोरता का अनुमान लगाने के लिए एक सामान्यीकृत गणितीय मॉडल को भी पेश किया गया है।

इस शोध प्रबंध में शोध के परिणाम वजन वहन करने वाले घुटने के जोड़ के एमआरआई को अधिक सुलभ बना सकते हैं। इसके अलावा, यह कार्य भारोत्तोलन एमआरआई के लिए नए अनुप्रयोग खोल सकता है और एमआरआई(MRI) घुटने की अनुसंधान में तेजी ला सकते हैं।

Table of Contents

CERTIFICATE.....	i
Acknowledgments	ii
Abstract.....	iv
संर 	vii
List of Abbreviations	xvii
List of Figures.....	xx
List of Tables	xxvii
Chapter 1	1
Introduction to the Thesis Content	1
1.1 Motivation Behind the Thesis	1
1.2 The Knee Joint Anatomy.....	3
1.2.1 Bones in the Knee Joint	4
1.2.2 Ligaments in the Knee Joint	5
1.2.3 Cartilage of the Knee Joint	6
1.2.4 Meniscus of the Knee Joint	8
1.2.5 Muscles of the Knee Joint	9
1.3 Knee Joint Movement and Its Axis	10

1.4 Imaging of the Knee Joint	12
1.5 MRI: History, basics, and applications	15
1.5.1 Historical Background of MRI	16
1.5.2 Basic of MRI	17
1.5.3 T ₁ and T ₂ relaxation Time	20
1.5.4 MRI Pulse Sequences	21
1.5.5 Knee Joint MRI	24
1.6 Clinical management of the knee joint.....	24
1.7 Simulation tools for knee joint modeling.....	25
1.8 Problem Addressed in the Thesis.....	26
1.8.1 Open-Standing MRI	26
1.8.2 Apparatus for Weight-bearing Knee MRI.....	27
1.9 Objectives.....	29
1.10 The Data Information and Image Acquisition Protocols	29
1.11 Outline of the Thesis	30
Chapter 2	33
Design and Development of Device for Axial Loading of the Knee Joint during MRI...33	
2.1 Introduction	34
2.1.1 Weight-bearing MRI and Need Assessment	34
2.1.2 Existing Solutions and Limitations.....	36
2.1.3 Objectives	36

2.2 Materials & Methods.....	37
2.2.1 Design and Development of Loading Device.....	37
2.2.2 Calibration of the Loading Device	45
2.2.3 MR Safety Assessment.....	47
2.2.4 The Device Induced Artifact Assessment	50
2.2.5 Device Ease of Using and Comfort Assessment	52
2.3 Results	53
2.3.1 Design and Development of a Knee Joint Axial Loading Device.....	53
2.3.2 Calibration of Elastic String	54
2.3.3 MR Safety Assessment.....	55
2.3.4 Assessment of Artifacts due to Loading Device	55
2.3.5 Ease of using and Degree of Comfort Assessment With the Device	56
2.4 Discussion	57
2.5 Conclusions	60
Chapter 3	61
Knee MR Quantitative Parameters Changes during Load.....	61
3.1 Introduction	62
3.2 Materials and Methods	65
3.2.1 Experiment Protocol and Image Acquisitions	65
3.2.2 Image Processing and Analysis	67
3.2.3 Statistical Analysis	71

3.4 Results	71
3.4.1 With Load versus Without Loading using 0.25 T MRI.....	71
3.4.2 With Load versus Without Load using 3.0 T MRI.....	74
3.5 Discussion	74
3.5.1 Limitations.....	76
3.6 Conclusions	77
Chapter 4	78
FEM Analysis on the Knee joint using Loading Device during MRI	79
4.1 Introduction	79
4.2 Methods.....	81
4.2.1 MRI Compatible Axial Loading Device	83
4.2.2 Image Acquisition.....	83
4.2.3 Bone Gap Measurement	85
4.2.4 Development of 3D-Model of the Knee Joint	85
4.2.5 Finite-Element-Analysis (FEA).....	88
4.2.6 Data Analysis.....	91
4.3 Results	92
4.3.1 Bone Gap Measurement	92
4.3.2 Femoral Cartilage Thickness: Rough versus Smoothen 3D Model	93
4.3.3 Finite-Element-Analysis.....	94
4.3.4 Estimation of Material Properties (Combined Compressive Stiffness).....	98

4.4 Discussions.....	100
4.4.1 Experimental Study	101
4.4.2 Simulation Study	101
4.4.3 Mathematical Model.....	102
4.4.5 Clinical Perspectives.....	104
4.4.6 Limitations.....	105
4.5 Conclusions	105
Chapter 5	107
Conclusion and Prospective Work	107
5.1 Conclusions of the thesis.....	108
5.2 Limitations	109
5.3 Future Scope of Work	110
5.3.1 Cartilage Segmentation: Automatic seed selection for radial search algorithms ..	112
5.3.2 Bone Segmentation: Region Growing Algorithms(RGA).....	113
5.3.3 Evaluation of Meniscus Deformation.....	114
Appendix-I.....	116
Reference	123
List Publications During My PhD	137
Awards During My PhD.....	140
About the Author	141

List of Abbreviations

50%BW	50% of body-weight
Δ mTFBG	Mean tibiofemoral bone gap difference
A	Anterior
ACL	Anterior cruciate ligament
AIC	Akaike Information Criterion
AICc	Akaike Information Criterion corrected
AL	Augmented Lagrange
ASTM	American Society for Testing and Materials
C	Central
CAD	Computer aided design
CCS	Combined-compressive-stiffness
CT	Computed Tomography
dGEMERIC	Delayed Gadolinium Enhanced MRI of Cartilage
ECE	Extracellular matrix
FASE	Fast-advanced-spin-echo
FCT	Femoral-cartilage-thickness
FCT2	Femoral-cartilage T ₂ -values
FEA	Finite-element-analysis
FEM	Finite-element-modeling
FFE	Fast-field-echo
FID	Free induction decay
FOV	Field of view
FSE	Fast-spin-echo
FS-PD	Fat-suppressed proton-density
FSPGR	Fat Saturated 3D-Fast Spoiled Gradient Echo
GF	Gravitational force
GRE/GE	Gradient-echo sequence
G _{ro}	Frequency gradient

G _{pe}	Phase encoding gradient
G _{ss}	Slice selective gradient
IE	Isotropic elastic
IEC	Institutional ethics committee
INR	Indian rupee
JSW	Joint space width
KL	Kellgren-Lawrence
LC	Lateral compartment
LCL	Lateral collateral ligaments
MC	Medial compartment
MCL	Medial collateral ligament
MF	Magnetic force
ML	Meniscal-length
MPC	Multi-Point Constraint
MR	Magnetic resonance
MRI	Magnetic resonance imaging
mTFBG	Mean tibiofemoral bone gap
NMR	Nuclear magnetic resonance
OA	Osteoarthritis
OCT	Optical coherence tomography
P	Posterior
PCG	Preconditioned conjugate gradients
PCL	Posterior cruciate ligament
PD-T ₂	Dual Proton Density-T ₂ -weighted
RF	Radio-frequency
RGA	Region growing algorithm
ROI	Region of interest
RPC	Relative percentage change
RSM	Radial-search method
SB45	Standing on both legs against gravity at 45° aligned
SB84	Standing on both legs against gravity at 84° aligned

SE	Spin-echo pulse sequence
SNR	Signal-to-noise ratio
SPGR	Spoiled-gradient-recalled-echo
SS84	Standing on a single leg against gravity at 84° aligned
SSIM	Structural similarity index measurement
STL	Standard Triangle Language
T	Tesla
TCT	Tibial-cartilage-thickness
TCT2	Tibial-cartilage-thickness
TE	Time of echo
TFBG	Tibiofemoral-bone-gap
TR	Time of repetition
WB-ST	Weight-bearing soft-tissue

List of Figures

Figure 1.1: Shows the knee joint compartments in fat-suppressed proton-density (FS-PD) MRI images. a) shows the patellofemoral compartment in the sagittal view of the knee joint, and b) shows the medial and lateral tibiofemoral compartments in the coronal view of the knee joint. MC and LC in b) represent medial condyle and lateral condyle, respectively.

Figure 1.2: A lateral view X-ray shows the knee from the side.

Figure 1.3: The knee joint's posterior view shows the cruciate ligaments and attachments.

Figure 1.4: A computer-aided model of the tibia, tibial cartilage, and meniscus in an isometric view. The figure depicts the wedge shape of the meniscus, which provides stability to the tibiofemoral articulation.

Figure 1.5: A sketch of the meniscus structure and its attachments. The figure depicts the difference in the size of medial and lateral ligaments, the attachment of meniscal horns, and the meniscus position of ACL and PCL attachments.

Figure 1.6: Shows quadriceps and hamstrings muscles in the anterior (left-hand side) and posterior (right-hand side) view of knee muscles.

Figure 1.7: Shows three arcs of flexion of a knee. This figure shows the axis of extension and flexion across the epicondyle of the femur bone.

Figure 1.8: The femur's translation motion during extension and flexion shows in the top view of the tibial profile.

Figure 1.9: Conventional MRI scanner of 3.0 Tesla Field Strength. (Courtesy: Mahajan Imaging Center, New Delhi)

Figure 1.10: The figure explains the MR physics with signal acquisition steps. a) bar magnet represents the dipole moment of nuclei, b) shows the random distribution of magnetic dipole moment in the absence of B_0 field. c) shows the magnetic moment vector aligned parallel or antiparallel to B_0 , in the presence of B_0 field. d) shows these magnetic moment vectors precess about B_0 field direction with a Larmor frequency (ω) and hence induce net magnetization or bulk magnetization (M_z) along the z-direction, whereas $M_{xy}=0$. e) shows the excitation stage with RF pulse of ' ω ', where net magnetization flips into the transverse plan and results in $M_{xy} \neq 0$. f) depict the recovery of longitudinal magnetization after the removal of RF pulse. g) represent the decay of M_{xy} due to the T_2 -relaxation process. h) shows the decay of the M_{xy} in a helical shape, i) shows the free induction decay curve of the induced signal ($S(t)$), and (j) shows the receiver coil perpendicular B_0 field.

Figure 1.11: Shows the T_1 and T_2 relaxation process graphs in a) and b), respectively.

Figure 1.12: Shows the sequence of events during scanning as a pulse sequence. a) shows a simple pulse sequence where events 1 to 5 are marked in a step manner. 1 switch on the slice select gradient (G_{ss}); then 2nd step switch on the 90° RF-pulse from transmitter coil as excitation stage; in step 3, phase encoding gradient (G_{pe}) trigger, and step 4 switch on the frequency encoding gradient/readout (G_{ro}) during free induction decay (5) acquired. b) represents the spin-echo sequences where 180° RF-pulse re-phases the M_{xy} magnetization, and the next echo's peak develops just after the TE time.

Figure 1.13: Represents the Gradient-echo sequence steps. Step 1 starts from the slice selection (G_{ss}), then 2 is the excitation step triggered by RF-pulse. The 3rd step is phase encoding by gradient coil (G_{pe}). Then in the 4th step, frequency encoding gradient (G_{ro}) first triggers negative polarity and turns to positive, and signal (5) is acquired during readout.

Figure 1.14: The block diagram of the workflow of the thesis; the figure shows the content of chapters of the thesis.

Figure 2.1: A CAD model of design-I, where a pulley is used to hang the weight against the waist belt, and the foot-rest acts as a plain ground to restrict the foot-sole to develop force equivalent to hanging weight.

Figure 2.2: A table-top design-II model, showing a big-wheel pulley that rotates to stretch the length of an elastic string.

Figure 2.3: Design-III demonstration on a volunteer. It shows the arrangement of elastic-string and waist-belt during knee loading condition.

Figure 2.4: Design-IV with a plain foot-rest and roller; a) shows the carpenter's work in modifying the design and b) shows the device in calibration setup with elastic string.

Figure 2.5: Design-V a) Drawing shows the mechanism of loading and arrangement of the device's components, b) shows the CAD model of the device's foot-rest connected with calf-rest by telescopic-channel, and c) shows the visuals of a subject put-on the device in laboratory setup outside MRI.

Figure 2.6: Design-VI a) shows the cushions incorporated in design-V, and b) shows the functioning of wedge-shaped knee flexion-angle-control, which keeps the knee in full extension during imaging. b) depicts the knee flexion angle with and without wedge-shape flexion-angle-control component.

Figure 2.7 Design-VII as an accessory, a) shows a visual of the device with accessory in the red dash lined box, and b) shows a CAD exploded view model of the design-VII with accessory in the red dash lined box.

Figure 2.8: Schematic of the experimental setup of calibration of elastic string

Figure 2.9: Schematic of the device with a subject to demonstrate the length measurement of elastic string 'x' and non-elastic string 'y'.

Figure 2.10: An experimental setup of MR-safety assessment, a) is a schematics of string suspension method experimental setup shows two forces act on the device to be tested as magnetic force(MF) and gravitational force(GF), and b) shows the visual of experimental setup where angular displacement of the device (with the influence of MF and GF) is measured by a protractor.

Figure 2.11: A setup of heat generation test for MR-safety; a) & b) shows the marked site on device and phantom to measure temperature, respectively, and c) shows visuals of the scanning of a phantom with the device.

Figure 2.12: An example of structural similarity index measurement (SSIM) map of with device and without device images.

Figure 2.13: Shows graph (with 95% confidence interval) of the stretched length of elastic belt vs applied load and fitted polynomial function.

Figure 3.1: A schematic diagram of experiment protocol of study-2a, where a) shows the subject scan in the supine position in a standing MRI, b) shows the subject's 45° aligned position with the ground during scanning, and c) shows the 84° aligned position of a subject during scanning. d) and e) show the experiment setup's visuals during scanning of study-2a and study-2b, respectively

Figure 3.2: Shows the method of meniscal extrusion measurement, where a) represents a schematic of meniscal measurement at a slice, and b) and c) meniscal measurement with slice selection method using axial oriented reconstructed knee images at the lateral and medial meniscal hoop, respectively.

Figure 3.3: Flow-chart of data processing for generating Tibiofemoral-bone-gap (TFBG), femoral-cartilage-thickness (FCT), tibial-cartilage-thickness (TCT), femoral-cartilage T_2 -values (FCT2), and tibial-cartilage T_2 (TCT2). (a) shows an overlay of a bone gap on the FSPGR image, (b) and (c) shows an overlay of cartilage-thickness on FS-PD and T2-W images, respectively. (d) and (e) show representative masks of bone gap, cartilage thickness, and (f) shows a map of cartilage T_2 values; the green arrows in (d) show the bone gap is evaluated normal to each pixel, red arrows in (e) represent the cartilage-thickness is evaluated tangential to each pixel, and red arrows in (f) show the cartilage T_2 -value is evaluated as tangentially average across each pixel; (g), (h), and (i) shows 2D-WearMaps for bone-gap, cartilage-thickness, and cartilage T_2 -values, respectively. Rectangular boxes on (g), (h), and (i) represent the whole lateral region (red-box), the entire medial region (red-dotted line) of each 2D-WearMap; lateral and medial regions of each 2D-WearMap where both cartilage contact with each other shows in yellow-box and yellow-dotted line, respectively.

Figure 3.4: Shows the flow of development of 2D-WearMap, a) shows the extraction of parameters from each slice, b) extracted parameters fed in a single image of 2D-WearMap, and c) shows the division of 2D-WearMap regions for averaging of parameters.

Figure 4.1: The stepwise workflow of the study is presented in the figure; Figure shows two phases of the study: experimental and simulation; $mTFBG$ is the mean tibiofemoral bone gap, $\Delta mTFBG$ is the difference between unloaded and loaded $mTFBG$

Figure 4.2: The stepwise processing of data. a) representative slice of 3D-FSPGR image of knee joint, b) segmented tissues (cartilage, bone, and meniscus) and overlaid on the grayscale MRI image, c), d) development phase of 3D surface geometry at MIMICS 20.0 and 3-MATIC Research 12.0, respectively, e) SpaceClaim platform used to convert STL files in the solid CAD model and assembly formation. f) Anterior and posterior view of mesh model. g) Zoom-in

anterior and posterior view to visualize the cartilage and meniscus, tibiofemoral bone gap, $\Delta mTFBG$ is the difference of unloaded and loaded $mTFBG$.

Figure 4.3. Comparison of a) rough 3D femoral cartilage model and b) finished 3D femoral cartilage model

Figure 4.4. Manual comparison of bonded and frictional contact region of rough and finished 3D model; a) Green and pink colour depict rough and smoothed 3D model of femur respectively; Region shown in figure with black boundary line is of femur-femoral cartilage bonded contact; b) Violet and grey colour depict rough and smoothed 3D model of femoral cartilage respectively; Region shown in figure with black boundary lines is of femoral cartilage-meniscus and femoral cartilage-tibial cartilage frictional contact.

Figure 4.5: a)–c) show bonded contacts, where a) femur with femoral-cartilage, b) tibia with the meniscus, and c) tibia with tibial-cartilage; Left-hand side shows contact bodies, and the right-hand side shows targeted bodies as opaque; d)–f) shows frictional contacts, d) tibial-cartilage with the meniscus, e) femoral-cartilage with the meniscus, and f) femoral-cartilage with tibial-cartilage; Left-hand side shows contact bodies, and the right-hand side shows targeted bodies as opaque.

Figure 4.6: Subject 1, Subject 1-Repeat, Subject 2, Subject 2-Repeat, Subject 3, and Subject 3-Repeat power function curve fitting graph for finite-element-analysis (FEA) simulated strain versus compressive stiffness of weight-bearing tibiofemoral soft-tissues shows in figure a)–f) respectively; g) shows 95% confidence interval estimation of all subject (All Graphs Developed in MATLAB R2018a).

Figure 4.7: The deformation profiles of each subject with the FEM model using various soft-tissue stiffness values.

Figure 4.8: *Effect on contact region during load with the shape of contact area, a) shows contact area remain same under load if contact region shape is plain surface, b) shows the increase in the area of contact region under applied load if contact region shape is curvature.*

Figure 5.1: *Showing the seed point selection for the radial search method.*

Figure 5.2: *Steps of meniscal FEM study*

List of Tables

Table 2.1: Experiment protocol of ease of using of put on and take-off of the loading device

Table 2.2: Observation table of degree of comfort experiment for the applied load using the loading device

Table 2.3: Results of ease of using of put-on and take-off of the loading device

Table 2.4: Observation table of degree of comfort experiment for the applied load using the loading device

Table 3.1: Experimental protocol of the study

Table 3.2: Observer variability of each segmented region of interest (ROI)

Table 3.3: Percentage changes in Tibiofemoral-bone-gap corresponding to the various condition of the loaded knee joint with respect to the rest position

Table 3.4: Changes in knee joint under load (50%BW) at 3.0 Tesla MRI

Table 4.1: Tibio-femoral bone gap measured without load and with load

Table 4.2: Mean femoral cartilage thickness of rough and smoothen 3D model

Table 4.3: Subject specific estimated combined compressive stiffness

Table 4.4: Percentage convergence error observed in each simulation